

Influence of nonuniform surface magnetic fields in wetting transitions in a confined two-dimensional Ising ferromagnet

Marta L. Trobo

Instituto de Física de Líquidos y Sistemas Biológicos (IFLYSIB), CCT-CONICET La Plata, UNLP, Calle 59 Nro. 789, (1900) La Plata, Argentina and Facultad de Ingeniería, Universidad Nacional de La Plata, Argentina

Ezequiel V. Albano

Instituto de Física de Líquidos y Sistemas Biológicos (IFLYSIB), CCT-CONICET La Plata, UNLP, Calle 59 Nro. 789, (1900) La Plata, Argentina and Facultad de Ciencias Exactas, Universidad Nacional de La Plata, Argentina

(Received 6 September 2013; published 15 November 2013)

Wetting transitions are studied in the two-dimensional Ising ferromagnet confined between walls where competitive surface fields act. In our finite samples of size $L \times M$, the walls are separated by a distance L , M being the length of the sample. The surface fields are taken to be short-range and nonuniform, i.e., of the form $H_1, \delta H_1, H_1, \delta H_1, \dots$, where the parameter $-1 \leq \delta \leq 1$ allows us to control the nonuniformity of the fields. By performing Monte Carlo simulations we found that those competitive surface fields lead to the occurrence of an interface between magnetic domains of different orientation that runs parallel to the walls. In finite samples, such an interface undergoes a localization-delocalization transition, which is the precursor of a true wetting transition that takes place in the thermodynamic limit. By exactly working out the ground state ($T = 0$), we found that besides the standard nonwet and wet phases, a surface antiferromagnetic-like state emerges for $\delta < -1/3$ and large fields ($H_1 > 3$), $H_1^{\text{tr}}/J = 3$, $\delta^{\text{tr}} = -1/3$, $T = 0$, being a triple point where three phases coexist. By means of Monte Carlo simulations it is shown that these features of the phase diagram remain at higher temperatures; e.g., we examined in detail the case $T = 0.7 \times T_{cb}$. Furthermore, we also recorded phase diagrams for fixed values of δ , i.e., plots of the critical field at the wetting transition (H_{1w}) versus T showing, on the one hand, that the exact results of Abraham [Abraham, *Phys. Rev. Lett.* **44**, 1165 (1980)] for $\delta = 1$ are recovered, and on the other hand, that extrapolations to $T \rightarrow 0$ are consistent with our exact results. Based on our numerical results we conjectured that the exact result for the phase diagram worked out by Abraham can be extended for the case of nonuniform fields. In fact, by considering a nonuniform surface field of some period λ , with $\lambda \ll M$, e.g., [$H_1(x, \lambda) > 0$], one can obtain the effective field H^{eff} at a λ coarse-grained level given by $H^{\text{eff}} = \frac{1}{\lambda} \sum_{x=1}^{\lambda} H_1(x, \lambda)$. Then we conjectured that the exact solution for the phase diagram is now given by $H^{\text{eff}}/J = F(T)$, where $F(T)$ is a function of the temperature T that straightforwardly follows from Abraham's solution. The conjecture was exhaustively tested by means of computer simulations. Furthermore, it is found that for $\delta \neq 1$ the nonwet phase becomes enlarged, at the expense of the wet one, i.e., a phenomenon that we call "surface nonuniformity-induced nonwetting," similar to the already known case of "roughness-induced nonwetting."

DOI: [10.1103/PhysRevE.88.052407](https://doi.org/10.1103/PhysRevE.88.052407)

PACS number(s): 68.08.Bc, 68.35.Rh, 64.60.De, 05.70.Fh

I. INTRODUCTION

When a liquid droplet is deposited onto a solid surface, it may spread across the surface such that the contact angle (Θ) is zero. This situation is called complete wetting. On the other hand, partial wetting occurs when $0 < \Theta < 180^\circ$, so that the droplet does not spread. Within this context we refer to a wetting transition as the surface phase transition that takes place from partial to complete wetting; for reviews on the topic see, e.g., Refs. [1–10].

The above scenario can easily be generalized in order to describe similar situations often encountered in condensed matter physics (i.e., from Bose-Einstein condensates [10] up to polymer blends [11]), a typical example being the localization-delocalization transitions, often observed in the confined Ising ferromagnet (for a review see, e.g., Ref. [12]) in $d = 2$ and 3 dimensions [13–36], which in turn are the precursors of true wetting transitions when the thermodynamic limit is properly taken [12,21,35,36]. Of course, wetting transitions are ubiquitous in both nature and technology; in fact, wetting occurs whenever a surface is exposed to a fluid or gas phase. Under these circumstances it is not

surprising that the study of wetting and related phenomena has attracted longstanding interest among both theorists and experimentalists [1–10]. Within this broad context it is worth mentioning that the surface structure can dramatically change wetting properties, and for this reason, the study of wetting in structured surfaces has become a hot topic of current research [9]. Recent advances in nano- and microtechnology [37–39] allows for the construction of patterned surfaces where wetting properties can be varied spatially in a controlled fashion, as well as structured surfaces such that the surface geometry can be controlled but the chemical structure is the same along the surface [9,40,41]. It is also known that surface roughness reinforces the wetting properties as compared to a smooth substrate; i.e., the effective contact angle is smaller when the roughness increases [42–44]. Conversely, the combined effects of roughness and heterogeneity can dramatically change the wettability of a surface leading, e.g., to superhydrophobicity [41]. One cannot, of course, forget examples from nature where a certain class of self-affine profiles of surface roughness occurring in some leaves may lead to macroscopic contact angles close to 180° , i.e., a nonwet situation known as

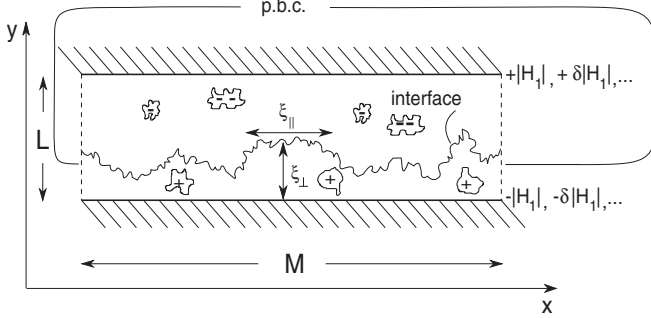


FIG. 1. Schematic description of the system geometry and its state slightly below the wetting transition temperature $T_w(H_1)$ such that ξ_{\parallel} and ξ_{\perp} are much larger than the lattice spacing. Here a nonuniform (positive) surface field acts on the upper wall, while a negative one acts on the lower wall. Notice that nonuniform surface fields are simply achieved by introducing a factor δ ($-1 \leq \delta \leq 1$), so that the strength of the field is given by $H_1, \delta H_1, H_1, \delta H_1, \dots$. By coarse graining the local magnetization on a length scale intermediate between the lattice spacing and ξ_{\perp} , one is left with one coarse-grained contour, i.e., an interface. Such an interface separates the domain with positive magnetization, which was assumed to be the majority domain at the top, without loss of generality, from the domain with negative magnetization at the bottom. So, in this particular example, the interface is still bound to the lower wall. Note that $\xi_{\parallel} \propto \xi_{\perp}$, and the mean distance of the interface from the nearest boundary is also of the same order as ξ_{\perp} . The choice of linear dimensions L , M , and of the periodic boundary conditions in the x direction (p.b.c.) is indicated.

“roughness-induced nonwetting” [45]. For that reason the understanding of wetting in (natural) leaves is relevant for the design and efficiency of pesticides.

Within this context the aim of this paper is to contribute to the understanding of the effects caused by surface heterogeneity on the wetting behavior just by addressing a simple case where the surface is geometrically uniform (flat) but chemical heterogeneity can be modeled by a suitable change in the interaction energy between different components of the surface and the fluid. For this purpose we will focus our study on the $d = 2$ confined Ising ferromagnet in the $L \times M$ ($L \ll M$) geometry, where at the confinement walls separated by a distance L nonuniform (short-range) surface magnetic fields act. In fact, it is well known that the $d = 2$ Ising magnet confined between antisymmetric walls (see Fig. 1) exhibits localization-delocalization transitions of the interface between domains of different orientation, which are the precursors of a true wetting transition occurring in the thermodynamic limit [12,21,35,36]. On the other hand, recent developments in a finite-size scaling theory [35,36] that rationalize wetting transitions in systems with short-range interactions between the walls and the system, as a bulk critical phenomenon with order parameter critical exponent $\beta = 0$, allow for a precise determination of the critical points and therefore, the construction of suitable phase diagrams.

The manuscript is organized as follows: in Sec. II we describe the geometry used in order to simulate the confined Ising ferromagnet, while Sec. III is devoted to a brief overview of recent improvements of the finite-size scaling theory for wetting. In Sec. IV we provide a brief description of the

simulation procedure, and our results are presented and discussed in Sec. V. Finally, we state our conclusions in Sec. VI.

II. THE CONFINED ISING FERROMAGNET

We consider the Hamiltonian of the Ising magnet in the $d = 2$ -dimensional square lattice in an $L \times M$ geometry, where each lattice site i carries a spin S_i that can take only two values, $S_i = \pm 1$ [21]. Periodic boundary conditions are assumed along the x direction, where the lattice is M rows long (see Fig. 1), while free boundary conditions are used in the y direction where the lattice is L files long. Furthermore, short-range nonuniform competitive surface fields $H_1(x)$ and $H_L(x)$ act on the first and last rows, respectively. Thus the Hamiltonian reads

$$\mathcal{H} = -J \sum_{(i,j)} S_i S_j - H_1(x) \sum_{i \in \text{row } 1} S_i - H_L(x) \sum_{i \in \text{row } L} S_i, \quad (1)$$

where $J > 0$ is the coupling constant between spins placed at nearest-neighbor sites, and the “surface fields” $H_1(x)$ and $H_L(x)$ act only on the spins placed in the first ($y = 1$) and last ($y = L$) rows, respectively (see Fig. 1). Notice that magnetic fields are measured in units of the coupling constant J .

For the study of wetting transitions, or more rigorously localization-delocalization “effective” transitions occurring in finite samples, it is convenient to adopt the antisymmetric situation $H_1(x) = -H_L(x) < 0$ and then consider the thermodynamic limit ($L \rightarrow \infty, M \rightarrow \infty$). Under these conditions actually two phase transitions are observed: one at the temperature T_{cb} that is the standard order-disorder critical temperature of the Ising magnet, namely, $\exp(\frac{2J}{k_B T_{cb}}) = \sqrt{2} + 1$, $T_{cb} \simeq 2.27J/k_B$ [46]. Furthermore a second wetting transition can be observed at $T_w(H_1) < T_{cb}$, and this wetting transition is of second order throughout the regime $0 < |H_1| < J$ if H_1 is taken uniform. Now, we further considered flat confinement walls, but the magnetic field is nonuniform adopting the values $H_1, \delta H_1, H_1, \delta H_1, \dots$ for adjacent sites along the walls. Here $-1 \leq \delta \leq 1$ is a parameter that allows us to control the degree of nonuniformity of the surface field. Of course, the case $\delta = 1$ (uniform field) corresponds to the standard case whose the phase diagram was worked out exactly by Abraham [13], such that the wetting transition occurs for H_{1w} given by the solution of

$$\exp \left[\frac{2J}{k_B T} \right] \left[\cosh \left(\frac{2J}{k_B T} \right) - \cosh \left(\frac{2H_{1w}}{k_B T} \right) \right] = \sinh \left(\frac{2J}{k_B T} \right). \quad (2)$$

It is worth mentioning that in a recent paper Fytas and Selke [47] have studied the role of interfacial adsorption in wetting transitions by using the three-state Blume-Capel model. In order to study wetting, these authors have employed special boundary conditions, modifying the exchange interaction at one of the boundaries by introducing, at one wall, the surface coupling αJ between the boundary spins and the neighboring bulk spins, with $0 \leq \alpha \leq 1$. Otherwise, the couplings between neighbors spins are always J . So in that approach the surface

field remains uniform but may be weakened in one wall, while in our study the factor δ is introduced in order to produce a nonuniform surface field.

III. BRIEF OVERVIEW OF THE FINITE-SIZE SCALING THEORY FOR CRITICAL WETTING WITH SHORT-RANGE SURFACE FIELDS

By taking the lattice spacing as the unit of length, the total number of spins is given by $N = L \times M$, and the magnetization m per lattice site can be evaluated as

$$m = \frac{1}{N} \sum_{i=1}^N S_i. \quad (3)$$

The thermal expectation $\langle |m| \rangle_T$ for $T < T_{cb}$ will be nonzero for the standard order-disorder transition. In contrast, for the wetting transition the total magnetization, or strictly speaking, its absolute value $\langle |m| \rangle_T$ undergoes a transition from nonzero value (corresponding to the presence of a localized interface between domains of opposite magnetization see Fig. 1) to zero just when the interface becomes delocalized at the effective wetting transition temperature, which can be obtained from simulation results in finite samples but must be extrapolated to the thermodynamic limit in order to obtain the true critical point. Based on these considerations, it has been proposed [35,36] that the distribution function $P_{L,M}(m)$ of the total magnetization in a finite geometry scales as [50,51]

$$P_{L,M}(m) = \xi_{\parallel}^{\beta/\nu_{\parallel}} \tilde{P} \left(\frac{L^{\nu_{\parallel}/\nu_{\perp}}}{M}, \frac{M}{\xi_{\parallel}}, m \xi_{\parallel}^{\beta/\nu_{\parallel}} \right), \quad (4)$$

an expression that generalizes the standard scaling law for isotropic systems having linear dimension L in all spatial directions [52], to the case with anisotropic correlation length exponents ν_{\parallel} and ν_{\perp} in the direction parallel and perpendicular to the interface (see Fig. 1), respectively. Now, the fact that M scales with ν_{\parallel} and L scales with ν_{\perp} can be used to show that the finite-size dependence on either L or M enters in the scaling function, through “the generalized aspect ratio” $c \equiv L^{\nu_{\parallel}/\nu_{\perp}}/M$, instead of the isotropic case where the “aspect ratio” L/M has to be used. The prefactor $\xi_{\parallel}^{\beta/\nu_{\parallel}}$ in Eq. (4) ensures that the probability distribution $P_{L,M}(m)$ can be properly normalized. Also, by taking suitable moments of $P_{L,M}(m)$ one can derive the following expressions:

$$\begin{aligned} \langle |m| \rangle &= \int_{-1}^1 dm |m| P_{L,M}(m) \\ &= \xi_{\parallel}^{-\beta/\nu_{\parallel}} \tilde{m} \left(\frac{L^{\nu_{\parallel}/\nu_{\perp}}}{M}, \frac{M}{\xi_{\parallel}} \right) \end{aligned} \quad (5)$$

and

$$\langle m^{2k} \rangle = \xi_{\parallel}^{-2k\beta/\nu_{\parallel}} \tilde{m}^{2k} \left(\frac{L^{\nu_{\parallel}/\nu_{\perp}}}{M}, \frac{M}{\xi_{\parallel}} \right), \quad (6)$$

$k = 1, 2, \dots$, where \tilde{m} and \tilde{m}^{2k} are scaling functions that do not need to be specified here. By using Eqs. (5) and (6) we can obtain the susceptibility χ given by

$$k_B T \chi = LM (\langle m^2 \rangle - \langle |m| \rangle^2), \quad (7)$$

and the Binder cumulant (U) given by

$$U(T) = 1 - \frac{\langle m^4 \rangle}{[3\langle m^2 \rangle^2]}, \quad (8)$$

which in turn are valuable observables in numerical simulations (see also below).

Note that for critical wetting in $d = 2$ dimensions there is a single independent critical exponent given by [48]

$$\nu_{\parallel} = 2. \quad (9)$$

Also, the hyperscaling relationship for interfacial phenomena $\nu_{\parallel} = 2 - \alpha_s$ [3] implies $\alpha_s = 0$ for the critical divergence of the surface specific heat. Furthermore, the correlation lengths describing the fluctuations of the interface scale as

$$\zeta_{\perp}^2 \propto \zeta_{\parallel}, \zeta_{\perp} \sim (T - T_w)^{-\nu_{\perp}}, \quad (10)$$

so that $\nu_{\perp} = 1$ [35,36]. Now, by pointing our attention to Eqs. (4)–(6), it follows that for a full scaling description of critical wetting in the $d = 2$ dimension one needs to fix the value of β . In recent papers [35,36] by using scaling arguments, we have shown that $\beta = 0$ for critical wetting with short-range forces. Of course, second-order transitions with an order parameter critical exponent equal to zero are rather unusual; see, e.g., Ref. [49] for a recent example. From the practical point of view the key results reviewed in this section, namely, $\beta = 0$, $\nu_{\parallel} = 2$ and $\nu_{\perp} = 1$ for critical wetting with short-range surface fields, imply that plots of the magnetization and all its moments obtained for different sample sizes will show a common intersection point provided that the “generalized aspect ratio” $c \equiv L^{\nu_{\parallel}/\nu_{\perp}}/M$ is kept constant. This intersection point allows for precise determinations of wetting transition points.

IV. BRIEF COMMENTS ON THE SIMULATION PROCEDURE

Monte Carlo simulations are performed by using the standard Metropolis algorithm since for systems below the critical temperature, exposed to boundary fields, cluster algorithms do not provide any advantage. As usual one Monte Carlo time step (MCS) involves $L \times M$ flipping attempts, so each spin of the sample is visited once, on average. Typically, we disregard 1×10^6 MCSs in order to allow for the equilibration of the system and subsequently, averages of relevant observables are taken over 5×10^6 MCSs. In this way the statistical error in relevant observables such as $\langle |m| \rangle$ and $\langle m^2 \rangle$ are of the order of the symbol size in the figures presented below. As expected, larger errors are observed in the evaluation of the cumulant, so that in many cases we used those measurements to qualitatively check the self-consistency of the data.

All simulations are performed for the choice $c = L^2/M = 9/8$ of the generalized aspect ratio, which on the one hand provides a suitable range for the observation of the common intersection point of the observables plotted as a function of temperature [35], and on the other hand allows for a set of integer solutions of L and M , i.e., values such as $(L, M) = (12, 128), (18, 288), (24, 512), (36, 1152)$, and $(48, 2048)$, which are commonly used in our calculations.

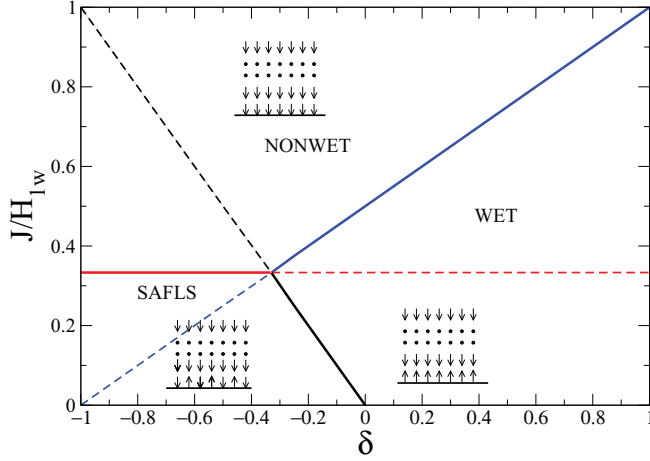


FIG. 2. (Color online) A phase diagram (J/H_{1w} vs δ) as obtained exactly for the ground state. Solid lines show the location of the various phase transitions according to Eqs. (16), (20), and (21), while the dashed lines correspond to unstable solutions of the equations. The sketch schematically shows the orientation of the spins in ground states analyzed in the text.

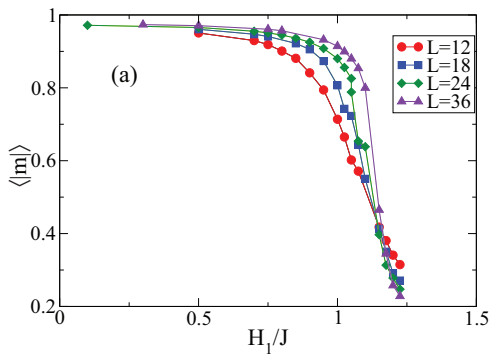
V. RESULTS AND DISCUSSION

A. A phase diagram (H_1 vs δ) for $T = 0$

In order to work out the phase diagram at $T = 0$, let us now evaluate the surface excess energy in the ground state for the following states: (a) nonwet surface-ordered, (b) wet surface-ordered, and (c) surface-covered for a sequence of up and down spins ($\uparrow\downarrow\uparrow\downarrow\uparrow\downarrow\uparrow\downarrow\dots$) according to the direction of the surface field ($\delta < 0$), in a surface antiferromagnetic-like state (SAFLS), while the bulk remains ordered. First, we assume a semi-infinite system with all spins in the bulk in the state $S_i = -1$ and a nonuniform surface magnetic field $H_1, \delta H_1, H_1, \delta H_1, \dots$, with $H_1 > 0$. Then the energy of the bulk is $H_{\text{Bulk}} = -2J$.

For case (a) the energy of the second layer is the same as in the bulk, while the first layer has energy

$$\mathcal{H}_A^{\text{1st}} = -\frac{3}{2}J + \frac{H_1}{2} + \frac{\delta H_1}{2}, \quad (11)$$



where in the first term we account for the missing neighbor spin at the surface, while the second term is due to the fact that the field $H_1(\delta H_1)$ is antiparallel (antiparallel or parallel depending on the sign of δ) to the spins in the first layer. So, by subtracting the bulk energy, the excess free energy of the nonwet surface-ordered state is

$$\Delta\mathcal{H}_A = \frac{1}{2}J + \frac{H_1}{2} + \frac{\delta H_1}{2}. \quad (12)$$

For case (b) the surface is wet, so all spins in the first layer are pointing up. Then the energy of the second layer is

$$\mathcal{H}_B^{\text{2nd}} = -J, \quad (13)$$

while for the first layer one has

$$\mathcal{H}_B^{\text{1st}} = -\frac{1}{2}J - \frac{H_1}{2} - \frac{\delta H_1}{2}. \quad (14)$$

Therefore, the excess energy is given by

$$\Delta\mathcal{H}_B = \frac{5}{2}J - \frac{H_1}{2} - \frac{\delta H_1}{2}. \quad (15)$$

Now, for the nonwet-wet transition one has $\Delta\mathcal{H}_A = \Delta\mathcal{H}_B$, so that

$$\frac{H_{1w}}{J} = \frac{2}{1 + \delta}. \quad (16)$$

From Eq. (16) one recovers the exact result for the ground state, namely, $H_{1w}/J = 1$ for $\delta = 1$ ($T = 0$); see also Eq. (2). Also, Eq. (16) suggests that for $\delta \rightarrow -1$ one would have $H_{1w} \rightarrow \infty$; however, this limit and values of $\delta < 1$ have to be investigated carefully. In fact, for state (c), one has that the surface adopts an antiferromagnetic-like state, so that the energy of the second layer is given by

$$\mathcal{H}_C^{\text{2nd}} = -\frac{3}{2}J, \quad (17)$$

while the first layer has energy

$$\mathcal{H}_C^{\text{1st}} = J - \frac{H_1}{2} + \frac{\delta H_1}{2}, \quad (18)$$

where we assumed that spins pointing up (down) are placed at sites with fields $H_1 > 0$ ($\delta H_1 < 0$). Then, the excess energy is given by

$$\Delta\mathcal{H}_C = \frac{7}{2}J - \frac{H_1}{2} + \frac{\delta H_1}{2}, \quad (19)$$

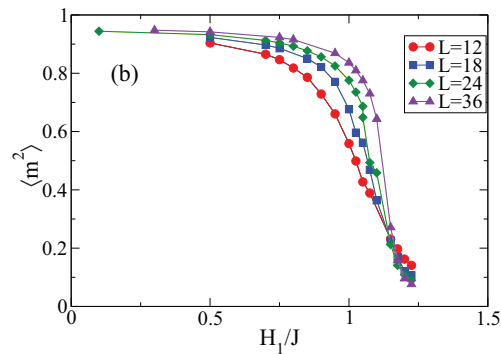


FIG. 3. (Color online) Plots of (a) the average absolute value of the magnetization $\langle |m| \rangle$ and (b) the magnetization square $\langle m^2 \rangle$ vs the surface field H_1/J . Results obtained for $\delta = 0.25$ and $T/T_{cb} = 0.7$. The different sample sizes used in the simulations, with a constant generalized aspect ratio $c = L^2/M = 9/8$, are indicated with different symbols.

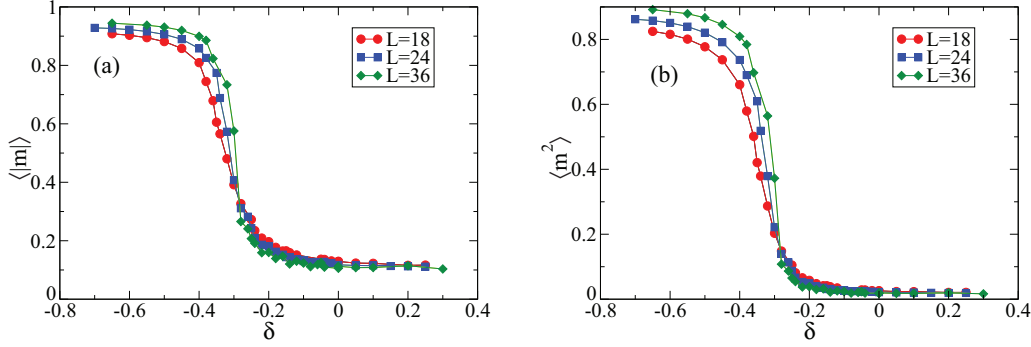


FIG. 4. (Color online) Plots of (a) the average absolute value of the magnetization $\langle |m| \rangle$ and (b) the magnetization square $\langle m^2 \rangle$ vs the parameter δ . Results obtained for $H_1/J = 3$ and $T/T_{cb} = 0.7$. The different sample sizes used in the simulations, with a constant generalized aspect ratio $c = L^2/M = 9/8$, are indicated with different symbols.

and for the nonwet SAFLS, one has that $\Delta H_A = \Delta H_C$ implies

$$\frac{H_{1w}}{J} = 3, \quad (20)$$

independent of δ . So, the SAFLS would prevail for $J/H_1 < 1/3$. However, for the wet SAFLS the solution of $\Delta H_B = \Delta H_C$ yields

$$\frac{H_{1w}}{J} = -\frac{1}{\delta}, \quad (21)$$

pointing out that the solution of Eq. (20) has an unstable branch for $\delta > -1/3$.

All these results [Eqs. (16), (20), and (21)] are summarized in Fig. 2, which shows the phase diagram corresponding to the ground state, i.e., plots of J/H_{1w} versus δ . It is worth mentioning that all phases coexist in a triple point given by $H_1^r/J = 3$, $\delta^r = -1/3$ ($T = 0$).

1. A phase diagram (H_{1w} vs δ) at finite temperature ($T/T_{cb} = 0.7$)

In order to evaluate the influence of the temperature on the phase diagram, shown in Fig. 2 for $T = 0$, it is necessary to perform extensive Monte Carlo simulations. For this purpose

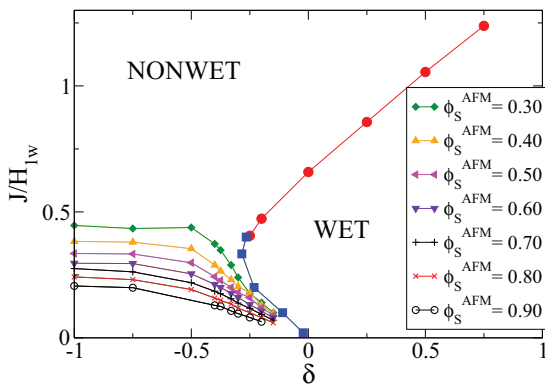


FIG. 5. (Color online) A phase diagram (J/H_{1w} vs δ) as obtained by means of Monte Carlo simulations for $T/T_{cb} = 0.7$. Data points obtained by scanning δ (H_1/J) by keeping H_1/J (δ) constant are shown by solid squares (circles). On the left-hand side and at the bottom we show seven “level” curves of the surface antiferromagnetic order parameter that covers the range $0.3 \leq \phi_S^{AFM} \leq 0.90$, as indicated.

we have chosen $T/T_{cb} = 0.7$, i.e., a temperature (far) below T_{cb} in order to be rid of undesired crossover effects due to bulk criticality, but high enough in order to ensure a reasonable flipping probability for the spins. Figure 3 shows plots of $\langle |m| \rangle$ and $\langle m^2 \rangle$ versus H_1/J as obtained for $\delta = 0.25$ and $T/T_{cb} = 0.7$. We observed a common intersection point of those observables, also including the cumulant (not shown here for the sake of space), which is obtained for samples of different size (but keeping the generalized aspect ratio $c = L^2/M = 9/8$ constant). This result confirms the scaling theory for wetting with short-range surface fields [35,36], as discussed in Sec. III. In fact, the theory predicts that by rationalizing the wetting transition in terms of a bulk order parameter (i.e. the magnetization) the corresponding order parameter critical exponent is $\beta = 0$ [35,36]. Consequently, the prefactors of the scaling functions of $\langle |m| \rangle$ and $\langle m^2 \rangle$ become independent of L as follows from Eqs. (5) and (6) (the prefactor of the cumulant is already independent of L), so that all those observables must exhibit a common intersection point at criticality. In this way we determine the critical point for the wetting transition given by $H_{1w}/J = 1.17 \pm 0.02$.

On the other hand, in order to locate the transition between nonwet phase with a SAFLS and the wet phase, close to the

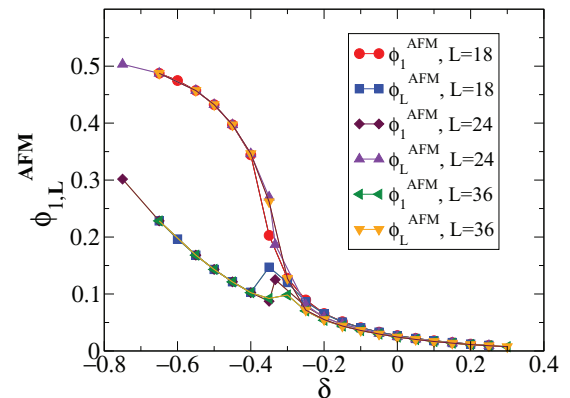


FIG. 6. (Color online) Plots of the AFM order parameters corresponding to the first (L th) row ϕ_1^{AFM} (ϕ_L^{AFM}) vs δ as obtained for $H_1/J = 3$ and $T/T_{cb} = 0.70$. The data correspond to three different lattice sizes, and the length of the corresponding walls are indicated. The generalized aspect ratio $C = L^2/M = 9/8$ is kept constant.

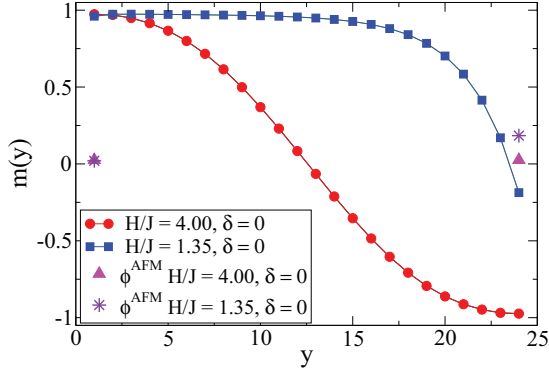


FIG. 7. (Color online) Plots of the magnetization profiles $m(y)$ vs the row index ($j = y$) as obtained for the nonwet phase (solid squares) with $H_1/J = 1.35$ and $\delta = 0$, as well as within the wet phase (solid circles) with $H_1/J = 4$ and $\delta = 0$. The values taken by the antiferromagnetic order parameters at the walls are also shown by the indicated symbols.

triple point, it is convenient to scan the parameter δ by keeping H_1/J constant, as shown in Fig. 4 for $\langle |m| \rangle$ and $\langle m^2 \rangle$. Again, for this case the common intersection point of the measured observables allows us to determine the critical point, e.g., $\delta_w = -0.27 \pm 0.02$, for $H_1/J = 3$ ($T/T_{cb} = 0.70$). Results obtained for the cumulant (not shown here for the sake of space) are in qualitative agreement. All points of the phase diagram obtained by scanning H_1/J and keeping $\delta = \text{constant}$ (by scanning δ and keeping H_1/J constant) are shown by full circles (squares) in Fig. 5.

In order to further characterize the SAFLS we evaluated the antiferromagnetic order parameter of rows $y = 1$ and $y = L$ given by ϕ_1^{AFM} and ϕ_L^{AFM} , respectively. Figure 6 shows plots of those observables versus δ as obtained for the same parameters as in Fig. 4, i.e., $H_1/J = 3$ and $T/T_{cb} = 0.70$. Here one observes that when the system is in the nonwet phase, ϕ^{AFM} adopts a large value at the wall where the interface is localized (e.g., since the interface can be attached to both walls with the same probability, we take ϕ_1^{AFM} for this case for the sake of clarity without losing generality). On the other hand, ϕ_L^{AFM} is rather negligible at the wall such that the interface is far away. By approaching the wetting phase one has that $\phi_1^{\text{AFM}} \approx \phi_L^{\text{AFM}}$, almost independent of the length M of the sample. Data points

that fulfill the above condition provide a rough estimation of the transition. It should be mentioned that in Fig. 6, close to the wetting transition, one observes jumps for ϕ_L^{AFM} for $L = 18$ (squares) and ϕ_1^{AFM} for $L = 24$ (diamonds), which are most likely due to excursions performed by the interface arriving close to the walls in those finite samples, affecting consequently the respective surface antiferromagnetic order parameters. This effect tends to vanish by increasing the sample size (see Fig. 6).

The transition between the nonwet state with a SAFLS and the wet phase is also evidenced by plotting magnetization profiles, i.e., plots of the magnetization versus the row index, as shown in Fig. 7. In fact, for the nonwet phase one has that the magnetization profile adopts the value of the bulk spontaneous magnetization along most of the rows, except for the last one ($y = L$), where the interface is bound to the wall. On the other hand, in the wet phase the profile is antisymmetric and falls almost linearly from a large positive value ($H_1 > 0$) to a large negative value ($H_1 < 0$), pointing out that the interface is fully delocalized with an average position close to the center of the strip ($y \approx L/2$). Also note that in Fig. 7 we show the values of both ϕ_1^{AFM} and ϕ_L^{AFM} for the sake of comparison: one has that $\phi_1^{\text{AFM}} \simeq \phi_L^{\text{AFM}} \simeq 0$ for the wet phase, while for the nonwet phase one has $\phi_1^{\text{AFM}} > 0$ and $\phi_L^{\text{AFM}} \simeq 0$ since in this particular example the interface is bound to the wall located at $y = L$.

The raw data shown in Figs. 3 and 4 are suitable to test the scaling behavior of the observables $\langle |m| \rangle$ and $\langle m^2 \rangle$, which follows from Eq. (6) and is generally given by

$$O(T, H_1, \delta) = \tilde{O} \left(\frac{L^{\nu_{\parallel}/\nu_{\perp}}}{M}, \epsilon M^{1/\nu_{\parallel}} \right), \quad (22)$$

for any observable O , where the scaling variable can be either $\epsilon_T = |(T - T_w)/T_{cb}|$, $\epsilon_{H_1} = (H_1 - H_{1w})/J$, or $\epsilon_{\delta} = \delta - \delta_w$. In fact, Figs. 8 and 9 show that data collapse is achieved by using $\nu_{\parallel} = 2$, $\nu_{\perp} = 1$, and $\beta = 0$, validating the scaling approach recently developed for wetting phenomena with short-range interactions between the walls and the system [35,36].

On the other hand, for large values of the surface field ($H_1/J \gg 3$) and $\delta \ll -1/3$ it is expected that the strongly antiferromagnetic surface layers attached to the walls of the sample would screen out the influence of surface fields on the bulk of the sample. In that case, the system would

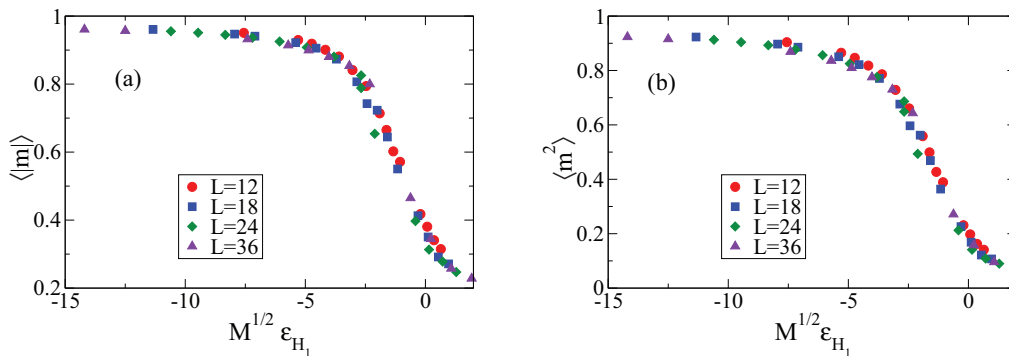


FIG. 8. (Color online) Scaling plots of the data shown in Fig. 3 for (a) the average absolute value of the magnetization $\langle |m| \rangle$ and (b) the magnetization square $\langle m^2 \rangle$ vs $M^{1/2} \epsilon_{H_1}$, with $\epsilon_{H_1} = (H_1 - H_{1w})/J$. Results obtained for $\delta = 0.25$ and $T/T_{cb} = 0.7$. The sample sizes used in the simulations, with a constant generalized aspect ratio $c = L^2/M = 9/8$, are indicated with different symbols.

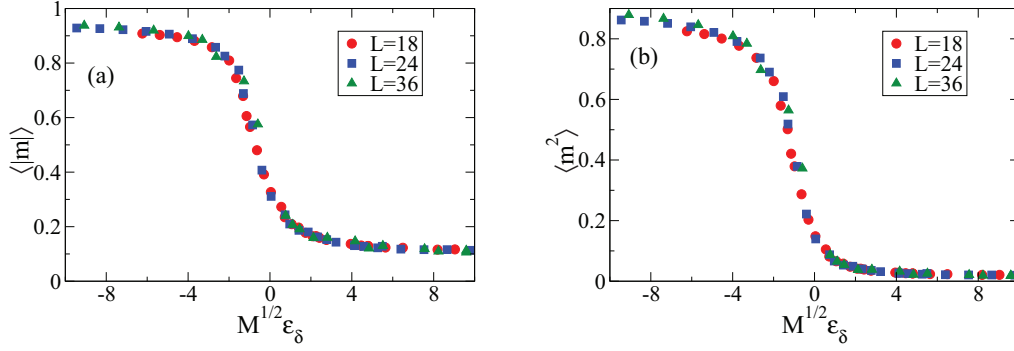


FIG. 9. (Color online) Scaling plots of the data shown in Fig. 4 for (a) the average absolute value of the magnetization $\langle |m| \rangle$ and (b) the magnetization square $\langle m^2 \rangle$ vs $M^{1/2} \epsilon_\delta$, with $\epsilon_\delta = \delta - \delta_w$. Results obtained for $H_1/J = 3$ and $T/T_{cb} = 0.7$. The sample sizes used in the simulations, with a constant generalized aspect ratio $c = L^2/M = 9/8$, are indicated with different symbols.

remain nonwet undergoing a genuine standard order-disorder transition when the temperature is increased. In order to avoid unpleasant crossover effects that may occur close to the transitions lines, we explored the above-discussed scenario deep inside the phase where the SAFLS prevails, i.e., for $H_1/J = 50$ and $\delta = -0.75$. For a standard order-disorder transition in the bulk, one recovers the isotropy in Eq. (4) with $\nu_{\parallel} = \nu_{\perp} = \nu = 1$ for the Ising model. Furthermore, one has $\beta = 1/8$, and Eq. (4) becomes [52]

$$P_{L,M}(m) = L^{-\beta/\nu} \tilde{P} \left(\epsilon L^{1/\nu}, \frac{L}{M} \right), \quad (23)$$

which means that data collapse of observables measured in finite samples of different size can be achieved only by keeping the geometric aspect ratio $c_G = L/M$ constant. In particular, the scaling behavior of the order parameter is given by

$$m(T, L, M) = L^{-\beta/\nu} \tilde{m} \left((T - T_{cb}) L^{1/\nu}, \frac{L}{M} \right). \quad (24)$$

Figures 10(a) and 10(b) show plots of $\langle |m| \rangle$ and U versus T as obtained for $H_1/J = 50$ and $\delta = -0.75$, by using samples of different size but keeping $c_G = 0.046875$ constant. The intersection point of the cumulant close to T_{cb} [10(b)] and the behavior of the magnetization [10(a)] fully support the

existence of a standard order-disorder transition of the bulk as a consequence of the screening effect of the SAFLS layers attached to the walls where the surface fields act. That statement is further confirmed by the data collapse observed in the insets of Fig. 10(a) and 10(b), which shows scaling plots of both the order parameter and the cumulant, respectively. Data collapse is achieved according to Eqs. (23) and (24), with $\nu = 1$ and $\beta = 1/8$ for the Ising model. As expected, we obtained a poor data collapse for the cumulant since our measurements of this observable are rather inaccurate, as was already discussed.

2. Wetting phase diagrams (H_1 vs T) and their dependence on δ

The phase diagram corresponding to uniform short-range surface fields is known exactly since the work of Abraham [13] and is given by Eq. (2). We further tested the scaling theory for critical wetting briefly discussed in Sec. III by determining few points for $\delta = 1$, which are in full agreement with the exact results [see Fig. 11(a)].

Subsequently we also evaluated the phase diagrams corresponding to different values of $\delta > 0$, e.g., $\delta = 1/4, 1/2$, and $3/4$. Figure 12 shows plots of $\langle |m| \rangle$ and $\langle m^2 \rangle$ versus T/T_{cb} as obtained for $\delta = 0.75$ and $H_1/J = 0.70$. From the

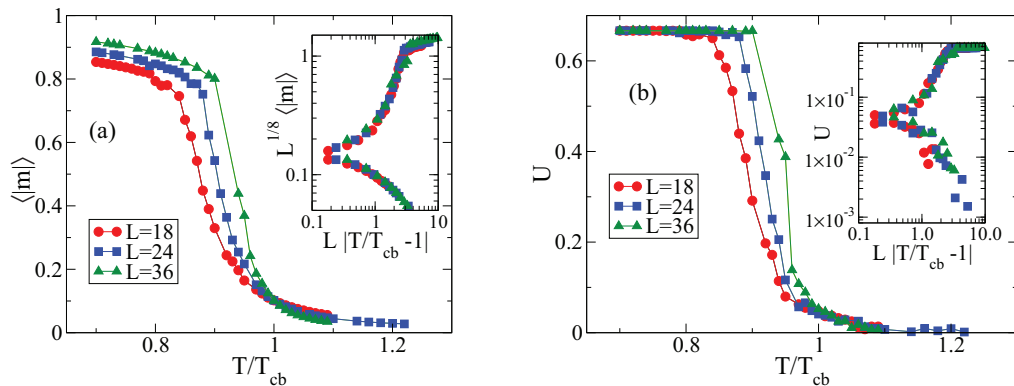


FIG. 10. (Color online) Plots of the average absolute value of (a) the magnetization $\langle |m| \rangle$ and (b) the cumulant U vs the temperature, for the choice $H_1/J = 50$ and $\delta = -0.75$. Data obtained for samples of different size as indicated by the symbols, but in all cases the geometric aspect ratio is $c_G = 0.046875$. The insets in (a) and (b) show the corresponding scaling plots [see Eqs. (23) and (24)], on a log-log scale, namely, $\langle |m| \rangle L^{1/8}$ and U vs $L(T/T_{cb} - 1)$, respectively.

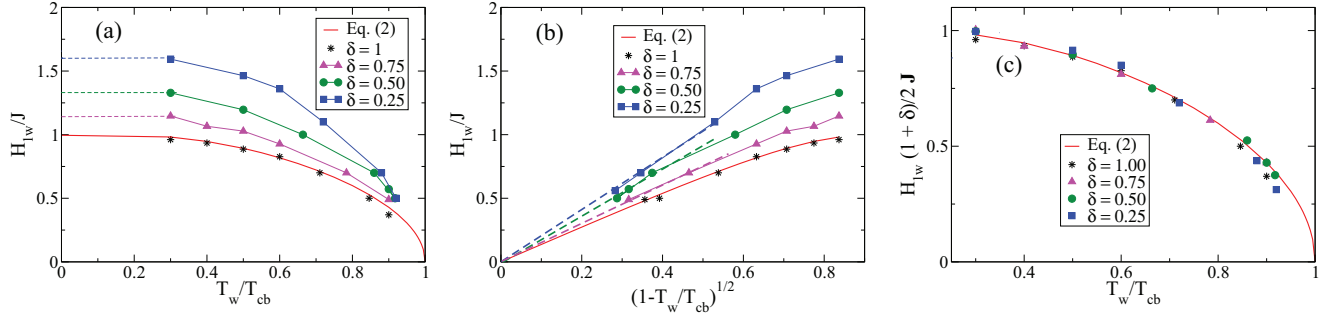


FIG. 11. (Color online) In all panels the full line corresponds to the exact solution given by Eq. (2). (a) Phase diagram (H_{1w}/J vs T_w/T_{cb}) as obtained for different values of δ as indicated. The solid line corresponds to the exact solution given by Eq. (2). The dashed lines in the low-temperature regime correspond to extrapolations to $T \rightarrow 0$ as obtained with Eq. (16). (b) Plot of $H_{1w}(T)/J$ vs $((T_{cb} - T)/T_{cb})^{1/2}$ as obtained by using the data shown in (a), showing that the exponent $\Delta_1 = 1/2$ holds [see Eq. (25)], irrespective of δ . Note that the dashed lines show extrapolations to $T \rightarrow T_{cb}$ drawn as a guide for the eye. (c) Plots of the critical wetting surface fields normalized by their ground state values [see Eq. (16) vs T_w/T_{cb}] as obtained by using the data shown in (a).

common intersection point of all observables one obtains $T_w/T_{cb} = 0.783 \pm 0.005$.

Furthermore, Fig. 13 shows that all these observables obey the expected scaling behavior obtained by taking $\beta = 0$, and $c = L^2/M = 1.125$ constant [see also Eq. (22)]. By repeating the above described procedure (plots not shown here for the sake of space) we drew phase diagrams for different values of δ [see Fig. 11(a)]. Here one observes that for low temperature the curves nicely extrapolate [dashed lines in Fig. 11(a)] to the exact values already calculated for the ground state, namely, $\frac{H_1}{J} = \frac{2}{1+\delta}$, as given by Eq. (16).

On the other hand, one aspect of wetting in the Ising model that attracted great attention is the behavior near bulk criticality. In fact, for a second-order wetting transition the inverse function $H_{1w}(T)$ of $T_w(H_1)$ behaves as [15]

$$H_{1w}(T) \propto (T_{cb} - T)^{\Delta_1}, \quad (25)$$

where Δ_1 is the critical exponent that controls the scaling behavior with the surface field H_1 near bulk criticality [53–55]. In $d = 2$ Abraham's exact solution [13] given by Eq. (2) implies $\Delta_1 = \frac{1}{2}$. Of course, for T close to T_{cb} we observed strong crossover effects due to the neighborhood of the standard order-disorder transition of the Ising ferromagnet, a fact that affects the accuracy of our determination of some wetting critical points. This shortcoming could be healed by

using even larger samples, but the task is beyond both the aim of this paper and our computational facilities. However, our data [see Fig. 11(b)] are consistent with the expected behavior irrespective of the value of the parameter δ .

B. A conjecture: Exact results for the phase diagram for nonuniform short-range fields

A simple view inspection of Fig. 11(a) suggests that by rescaling the critical wetting field by the corresponding result of the ground state [see Eq. (16)], one may obtain data collapse for different values of δ . That assumption is nicely verified in Fig. 11(c), which leads us to conjecture that the exact solution of the phase diagram for short-range nonuniform fields can straightforwardly be derived from the result of Abraham [Eq. (2)] simply by rescaling the surface field. In fact, by applying some algebra to Eq. (2) one obtains the temperature dependence of the critical wetting field, namely,

$$\begin{aligned} H_{1w}(T)/J &= (k_B T/2J) \cosh^{-1}[\cosh(2J/k_B T) \\ &\quad - \sinh(2J/k_B T) \exp(-2J/k_B T)] \\ &\equiv F(T). \end{aligned} \quad (26)$$

Now, if a nonuniform surface field is applied at the confinement walls we conjecture that the exact solution for

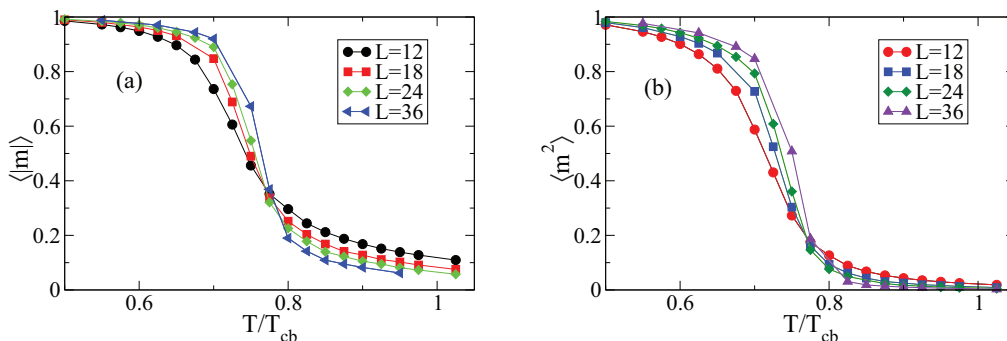


FIG. 12. (Color online) Plots of (a) the average absolute value of the magnetization $\langle |m| \rangle$ and (b) the magnetization square $\langle m^2 \rangle$ vs T/T_{cb} , for the choice $H_1/J = 0.70$ and $\delta = 0.75$. From the common intersection point of both observables, one concludes that $T_w/T_{cb} = 0.783 \pm 0.005$.

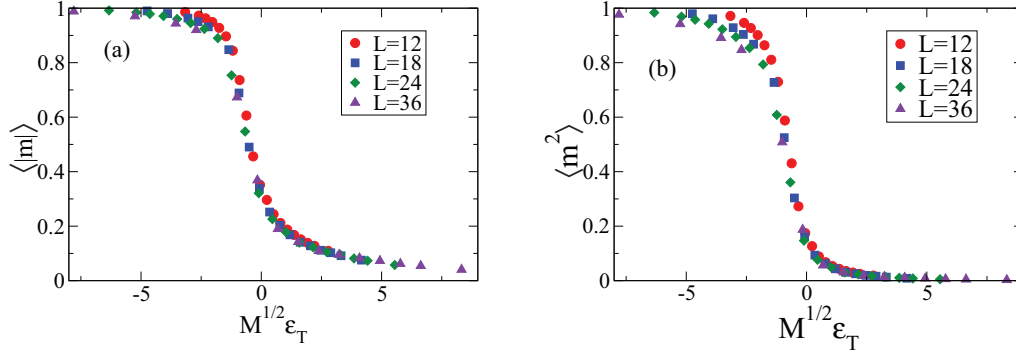


FIG. 13. (Color online) Scaling plots of (a) $\langle |m| \rangle$ and (b) $\langle m^2 \rangle$ vs $\epsilon_T \sqrt{M}$ as obtained by using the data already shown in Fig. 11, which were obtained for $H_1/J = 0.70$, $\delta = 0.75$, and various choices of the system size (for $L^2/M = 9/8$).

the phase diagram is given by

$$H_w^{\text{eff}}/J = F(T), \quad (27)$$

where H^{eff} is an effective surface field that has to be evaluated, e.g., as a function of the original nonuniform field, by working out the ground state solutions. In fact, by considering a nonuniform field of some period $\lambda \ll M$, such that $H_1(x, \lambda) > 0$, one can avoid the formation of SAFLS layers at the walls and the effective field H^{eff} at a λ coarse-grained level is given by a simple average, namely,

$$H^{\text{eff}} = \frac{1}{\lambda} \sum_{i=1}^{\lambda} H_i(x, \lambda). \quad (28)$$

In the particular case of the nonuniform field used in this paper one has that H^{eff} can be evaluated according to Eq. (28) for the wet-nonwet transition. However, due to the subtle behavior of the spin layers attached to the walls for $\delta < 0$, the transitions involving the SAFLS require the knowledge of the ground state solutions for the calculation of the effective field. In this way we obtained

$$H_w^{\text{eff}}/J = \begin{cases} \frac{2}{1+\delta} F(T) & \text{for } -1/3 < \delta < 1, \text{ wet-nonwet} \\ \frac{-1}{\delta} F(T) & \text{for } -1/3 < \delta < 0, \text{ wet-SAFLS} \\ 3F(T) & \text{for } -1 < \delta \leq -1/3, \text{ nonwet-SAFLS.} \end{cases} \quad (29)$$

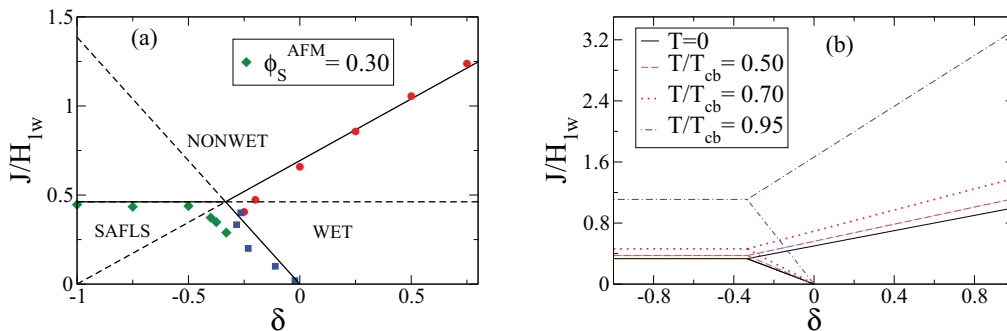


FIG. 14. (Color online) (a) Phase diagram, J/H_{1w} vs δ obtained for $T/T_{cb} = 0.70$. The solid circles and squares correspond to the numerical data already shown in Fig. 5. Also, the solid diamonds show the level curve corresponding to $\phi_S^{\text{AFM}} = 0.30$, which is used in order to give insight into the location of the SAFLS. Solid lines correspond to the exact solution given by Eq. (29), while the dashed lines are unstable branches. (b) Phase diagrams obtained at different temperatures by using Eq. (29). Note that at the triple point the value of $\delta = -1/3$ remains unchanged irrespective of T . Also note that only the stable solutions are shown for the sake of clarity.

Figure 14(a) shows a comparison between the phase diagram (J/H_{1w} vs δ) corresponding to $T/T_{cb} = 0.70$ as obtained numerically and by means of Eq. (29). Here we observe excellent agreement for $\delta \geq -0.2$, i.e., when it is accurate to determine critical points by using numerical data obtained by scanning $H_1(\delta)$ keeping δ (H_1) constant. Note that the accuracy of our numerical data decreases close to the triple point at $\delta = -1/3$. This effect is probably due to the contributions of many sources, among others: the missing of entropic contributions in Eq. (29) that is based in ground state considerations, the onset of the formation of the SAFLS, the missing of corrections to scaling affecting our relatively small samples, etc. Also, and for the sake of comparison, in Fig. 14(a) we include the points corresponding to $\phi_S^{\text{AFM}} = 0.30$ that are very close to the exact results. Of course, the location of the SAFLS by means of numerical simulations is no longer straightforward, but our data provide a rough estimation. For the sake of completeness, in Fig. 15 we show phase diagrams, i.e., plots of H_{1w}/J versus T/T_{cb} , as obtained by means of Eq. (29) and using different values of δ . It is found that, irrespective of the value of the parameter δ that controls the degree of nonuniformity of the surface field, the nonwet phase is always enhanced at the expense of the wet one. The enhancement of the nonwet phase due to the increment of the surface roughness is a well-documented phenomenon called “roughness-induced nonwetting,” the behavior of water drops

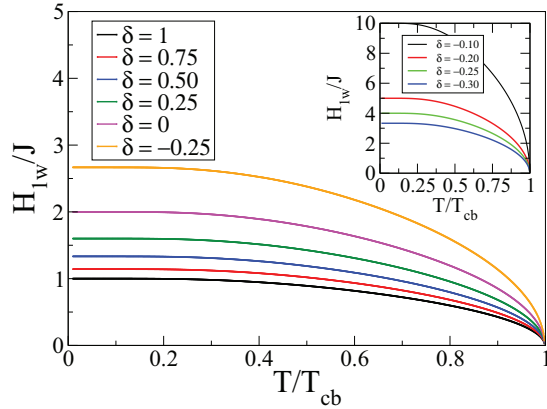


FIG. 15. (Color online) Plots of H_{1w}/J vs T/T_{cb} , as obtained by means of Eq. (29) and using different values of δ . The main panel corresponds to the case $\delta > 0$, while the inset shows results obtained for $\delta < 0$. Note that in all cases $\delta \neq 1$ causes the enhancement of the nonwet phase as compared with the case of the uniform field that is recovered for $\delta = 1$.

on some natural leaves being a paradigmatic example [45]. In the same direction, our observation can be considered as an example of similar characteristics, namely, “surface nonuniformity induced nonwetting.” This phenomenon is dominant for negative values of δ , and in particular for $\delta < -1/3$ the wetting phase is no longer observed.

VI. CONCLUSIONS

Our numerical study of the two-dimensional Ising ferromagnet confined between walls, where competitive (nonuniform) surface fields act, confirms the validity of the

recently proposed scaling theory for critical wetting transitions [35,36], which rationalizes these transitions in terms of a bulk critical phenomenon with an order parameter critical exponent $\beta = 0$. By considering a surface field of the form $H_1, \delta H_1, H_1, \delta H_1, \dots$, where the parameter $-1 \leq \delta \leq 1$ allows us to control the nonuniformity of the fields, we exactly work out the ground state phase diagram, i.e., H_{1w} versus δ . In this way, apart from the standard wet and nonwet phases, we also identify a surface antiferromagnetic-like state that prevails for $\delta < -1/3$ and $H_1 > 3$, so that the system exhibits a triple point. We also calculate that phase diagram by means of numerical simulations for higher temperatures, showing that it preserves its main features. Of course, the standard phase diagram of wetting phenomena, i.e., plot of H_{1w} versus T , is also evaluated by taking δ as a parameter. Based on the obtained numerical results we conjecture that the exact solution due to Abraham [13] could be generalized for a certain class of nonuniform surface fields when they can be replaced by an effective field obtained by means of a suitable coarse graining over a certain finite range.

We find that the nonuniformity of the surface fields causes the enhancement of the nonwet phase, i.e., a phenomenon that we call “surface nonuniformity-induced nonwetting.” We expect that our results will contribute to the understanding of the role played by surface heterogeneity in wetting phenomena, which is a relevant topic from both the basic and applied points of view that deserves further studies.

ACKNOWLEDGMENTS

This work was supported by CONICET through PIP 143 and the Universidad Nacional de La Plata, Argentina. E.V.A. thanks K. Binder for useful discussions.

-
- [1] J. S. Rowlinson and B. Widom, *Molecular Theory of Capillarity* (Oxford University Press, Oxford, 1982).
- [2] D. E. Sullivan and M. M. Telo da Gama, in *Fluid Interfacial Phenomena*, edited by C. Croxton (Wiley, New York, 1986), p. 45.
- [3] S. Dietrich, in *Phase Transitions and Critical Phenomena*, edited by C. Domb and J. L. Lebowitz, Vol. 12 (Academic, London, 1988), p. 1.
- [4] M. Schick, in *Liquids at Interfaces*, edited by J. Charvolin, J.-F. Joanny, and J. Zinn-Justin (Elsevier, Amsterdam, 1990), p. 415.
- [5] D. Bonn and D. Ross, *Rep. Progr. Phys.* **64**, 1085 (2001).
- [6] P. G. De Gennes, F. Brochard-Wyart, and D. Quéré, *Capillarity and Wetting Phenomena: Drops, Bubbles, Pearls, Waves* (Springer, Berlin, 2003).
- [7] M. Schön and S. Klapp, *Nanoconfined Fluids: Soft Matter between Two and Three Dimensions* (John Wiley & Sons, New York, 2006).
- [8] D. R. Clarke, M. Rühle, and A. P. Tomsia (eds.), *Low and High Temperature Wetting: State of the Art; Annual Review of Materials Research*, Vol. 38 (Annals Reviews, Palo Alto, CA, 2008).
- [9] D. Bonn, J. Eggers, J. O. Indekeu, J. Meunier, and E. Rolley, *Rev. Mod. Phys.* **81**, 739 (2009).
- [10] J. O. Indekeu, *Phys. A* **389**, 4332 (2010).
- [11] M. Müller and K. Binder, *J. Phys.: Condens. Matter* **17**, S333 (2005).
- [12] K. Binder, D. P. Landau, and M. Müller, *J. Stat. Phys.* **110**, 1411 (2003).
- [13] D. B. Abraham, *Phys. Rev. Lett.* **44**, 1165 (1980).
- [14] M. E. Fisher and H. Nakanishi, *J. Chem. Phys.* **75**, 5857 (1981).
- [15] H. Nakanishi and M. E. Fisher, *Phys. Rev. Lett.* **49**, 1565 (1982).
- [16] H. Nakanishi and M. E. Fisher, *J. Chem. Phys.* **78**, 3279 (1983).
- [17] K. Binder, D. P. Landau, and D. M. Kroll, *Phys. Rev. Lett.* **56**, 2272 (1986).
- [18] D. B. Abraham and E. R. Smith, *J. Stat. Phys.* **43**, 621 (1986).
- [19] K. Binder and D. P. Landau, *Phys. Rev. B* **37**, 1745 (1988).
- [20] K. Binder, D. P. Landau, and S. Wansleben, *Phys. Rev. B* **40**, 6971 (1989).
- [21] E. V. Albano, K. Binder, D. W. Heermann, and W. Paul, *Surf. Sci.* **223**, 151 (1989).
- [22] E. V. Albano, K. Binder, D. W. Heermann, and W. Paul, *J. Stat. Phys.* **61**, 161 (1990).

- [23] A. O. Parry and R. Evans, *Phys. Rev. Lett.* **64**, 439 (1990).
- [24] A. O. Parry and R. Evans, *Physica A* **181**, 250 (1992).
- [25] K. Binder, D. P. Landau, and A. M. Ferrenberg, *Phys. Rev. Lett.* **74**, 298 (1995).
- [26] K. Binder, D. P. Landau, and A. M. Ferrenberg, *Phys. Rev. E* **51**, 2823 (1995).
- [27] K. Binder, R. Evans, D. P. Landau, and A. M. Ferrenberg, *Phys. Rev. E* **53**, 5023 (1996).
- [28] A. Maciolek and J. Stecki, *Phys. Rev. B* **54**, 1128 (1996).
- [29] A. Maciolek, *J. Phys. A* **29**, 3837 (1996).
- [30] E. Carlon and A. Drzewinski, *Phys. Rev. E* **57**, 2626 (1998).
- [31] E. V. Albano, K. Binder, and W. Paul, *J. Phys.: Condens. Matter* **12**, 2701 (2000).
- [32] A. De Virgiliis, E. V. Albano, M. Müller, and K. Binder, *Phys. A* **352**, 477 (2005).
- [33] B. J. Schulz, K. Binder, and M. Müller, *Phys. Rev. E* **71**, 046705 (2005).
- [34] L. Pang, D. P. Landau, and K. Binder, *Phys. Rev. Lett.* **106**, 236102 (2011).
- [35] E. V. Albano and K. Binder, *Phys. Rev. E* **85**, 061601 (2012).
- [36] E. V. Albano and K. Binder, *Phys. Rev. Lett.* **109**, 036101 (2012).
- [37] G. Decker and J. B. Schlenoff (eds.), *Multilayer Thin Films: Sequential Assembly of Nanocomposite Materials* (Wiley-VCH, Weinheim, 2002).
- [38] Y. Champion and H.-J. Fecht (eds.), *Nano-Architected and Nano-Structured Materials* (Wiley-VCH, Weinheim, 2004).
- [39] S. Zhang (ed.), *Handbook of Nanostructured Thin Films and Coatings*, Vols. 1–3 (CRC Press, Boca Raton, FL, 2010).
- [40] S. Dietrich, M. N. Popescu, and M. Rauscher, *J. Phys.: Condens. Matter* **17**, S577 (2005).
- [41] D. Quéré, *Rep. Prog. Phys.* **68**, 2495 (2005).
- [42] C. Borgs, J. De Coninck, R. Kotecky, and M. Zinque, *Phys. Rev. Lett* **74**, 2292 (1995).
- [43] P. Swain and R. Lipowsky, *Langmuir* **14**, 6772 (1998).
- [44] J. De Coninck, J. Ruiz, and S. Miracle-Sole, *Phys. Rev. E* **65**, 036139 (2002).
- [45] S. Herminghaus, *Europhys. Lett.* **52**, 165 (2000).
- [46] L. Onsager, *Phys. Rev.* **65**, 117 (1944).
- [47] N. G. Fytas and W. Selke, *Eur. Phys. J. B* **86**, 365 (2013).
- [48] D. B. Abraham, in C. Domb and J. L. Lebowitz (eds.), *Phase Transitions and Critical Phenomena*, Vol. 10 (Academic, London, 1986), p. 1.
- [49] L. D. C. Jaubert, J. T. Chalker, P. C. W. Holdsworth, and R. Moessner, *Phys. Rev. Lett.* **105**, 087201 (2010).
- [50] K. Binder and J. S. Wang, *J. Stat. Phys.* **55**, 87 (1989).
- [51] K. Binder, in *Finite Size Scaling and Numerical Simulation of Statistical Systems*, edited by V. Privman (World Scientific, Singapore, 1990), p. 173.
- [52] K. Binder, *Phys. Rev. Lett.* **47**, 693 (1981).
- [53] K. Binder and P. C. Hohenberg, *Phys. Rev. B* **6**, 3461 (1972).
- [54] K. Binder and P. C. Hohenberg, *Phys. Rev. B* **9**, 2194 (1974).
- [55] K. Binder, in *Phase Transitions and Critical Phenomena*, edited by C. Domb and J. L. Lebowitz, Vol. 8 (Academic, London, 1983), p. 1.